

# Csf1r<sup>-</sup> macrophages govern the second wave of neutrophils for bone repair

Zhifeng He<sup>1†</sup>, Linan Shi<sup>2†</sup>, Yuko Nakamichi<sup>1</sup>, Kohei Murakami<sup>3</sup>, Toshihide Mizoguchi<sup>4</sup>, Yuki Matsushita<sup>5</sup>, Hirotaka Matsumoto<sup>6</sup>, Shinichirou Ito<sup>7</sup>, Shunsuke Uehara<sup>8</sup>, Rina Iwamoto<sup>1</sup>, Takumi Takahashi<sup>1</sup>, Zizhao Tian<sup>9</sup>, Toru Hiraga<sup>10</sup>, Ruoxuan Li<sup>1</sup>, Masataka Kasahara<sup>7</sup>, Kazuo Okamoto<sup>11</sup>, Hiroshi Takayanagi<sup>12</sup>, Martin M Matzuk<sup>13</sup>, Nobuyuki Udagawa<sup>8</sup>, Yasuhiro Kobayashi<sup>1\*</sup>

<sup>1</sup>Department of Hard Tissue Research, Institute for Oral Science, Matsumoto Dental University  
<sup>2</sup>Department of Stomatology, Affiliated Hangzhou First People' s Hospital, School of Medicine, Westlake University,  
<sup>3</sup>Department of Veterinary Immunology, Okayama University of Science,  
<sup>4</sup>Institute for Oral Science, Tokyo Dental College,  
<sup>5</sup>Department of Skeletal Development and Regenerative Biology, Nagasaki University Graduate School of Biomedical Sciences,  
<sup>6</sup>School of Information and Data Science, Nagasaki University,  
<sup>7</sup>Department of Pharmacology, Tokyo Dental College,  
<sup>8</sup>Department of Biochemistry, Matsumoto Dental University,  
<sup>9</sup>Department of Biomedical Sciences, City University of Hong Kong,  
<sup>10</sup>Department of Histology and Cell Biology, Matsumoto Dental University,  
<sup>11</sup>Cancer Research Institute, Division of Immune Environment Dynamics, Kanazawa University,  
<sup>12</sup>Department of Immunology, Graduate School of Medicine, The University of Tokyo,  
<sup>13</sup>Department of Pathology& Immunology and Center for Drug Discovery, Baylor College of Medicine,

†These authors contributed equally to this work.

- 27    \*Corresponding author
- 28    E-mail address: yasuhiko.kobayashi@mdu.ac.jp
- 29    1780 Hiro-oka Gobara, Shiojiri, Nagano 399-0781, Japan
- 30    Tel: +81-263-51-2238, Fax: +81-263-51-2223

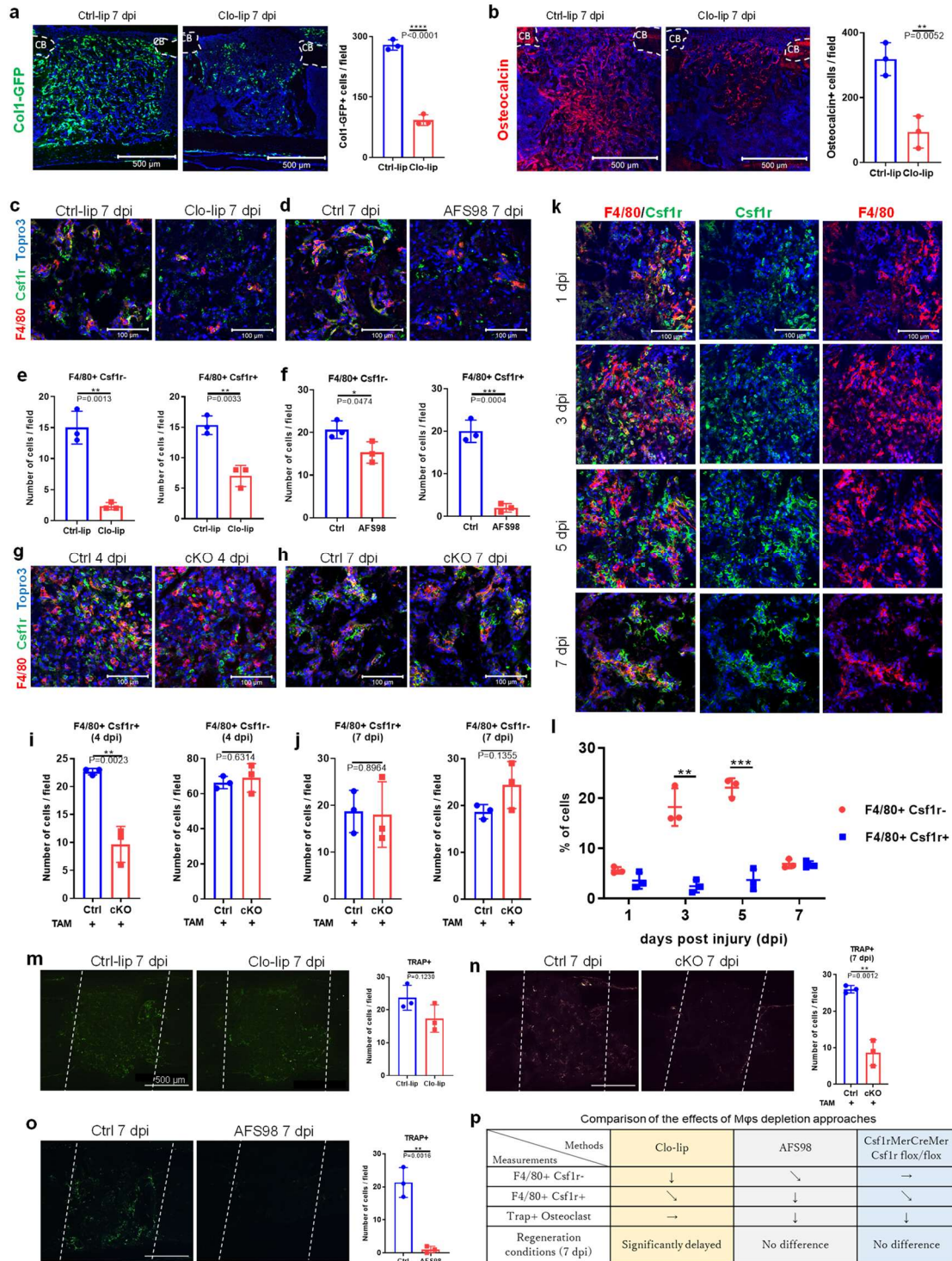


**Figure. S1 Mφ subpopulations distinguished by F4/80 and Csf1r expression, and osteoclasts targeted by various depletion strategies.**

**(a)** Immunofluorescent analysis of *Col1*-GFP(+) cells at the bone injury site at 7 dpi, n = 3.

**(b)** Immunofluorescent analysis of osteocalcin(+) cells at the bone injury site at 7 dpi, n = 3.

**(c- f)** Immunofluorescent analysis of F4/80(+)Csf1r(+) and F4/80(+)Csf1r(–) cells at the bone injury sites at 7 dpi from Ctrl-lip or Clo-lip-treated (**c, e**), and AFS98 or saline-treated mice (**d, f**), n = 3.

**(g- j)** Immunofluorescent analysis of F4/80(+)Csf1r(+) and F4/80(+)Csf1r(–) cells at the bone injury site at 4 and 7 dpi in *Csf1r*<sup>MerCreMer</sup>; *Csf1r*<sup>fl/fl</sup> and control mice (genotypes of control mice: Cre<sup>–</sup>, Cre<sup>+/+</sup>, Cre<sup>fl/+</sup>), n = 3.

**(k)** Immunofluorescent analysis of F4/80(+)Csf1r(+) and F4/80(+)Csf1r(–) cells at the bone injury sites at 1, 3, 5 and 7 dpi.

**(l)** Percentage of F4/80(+)Csf1r(+) and F4/80(+)Csf1r(–) cells at the bone injury sites at 1, 3, 5 and 7 dpi, n = 3.

**(m- o)** TRAP staining using the ELF 97 phosphatase substrate of the bone injury sites at 7 dpi by macrophage depletion methods using Clo-lip (**m**), macrophage-lineage cell specific deletion of the *Csf1r* gene (**n**), and AFS98 (**o**), n = 3. The region between the two dash lines indicates the injury site.

**(p)** Summary of Figure 1 and Fig. S1: The effects of three Mφ depletion strategies (Clo-lip, AFS98, and *Csf1r* conditional knockout) on F4/80(+)Csf1r(–), F4/80(+)Csf1r(+) cell faction, and osteoclasts, as well as bone regeneration outcomes. Scale bars with its value are shown in each image. Data are shown in mean± S.D. Statistical significance was determined by unpaired Student's t-tests. P- values are shown in each graph (\*\*: p < 0.01; \*\*\*: p < 0.001).

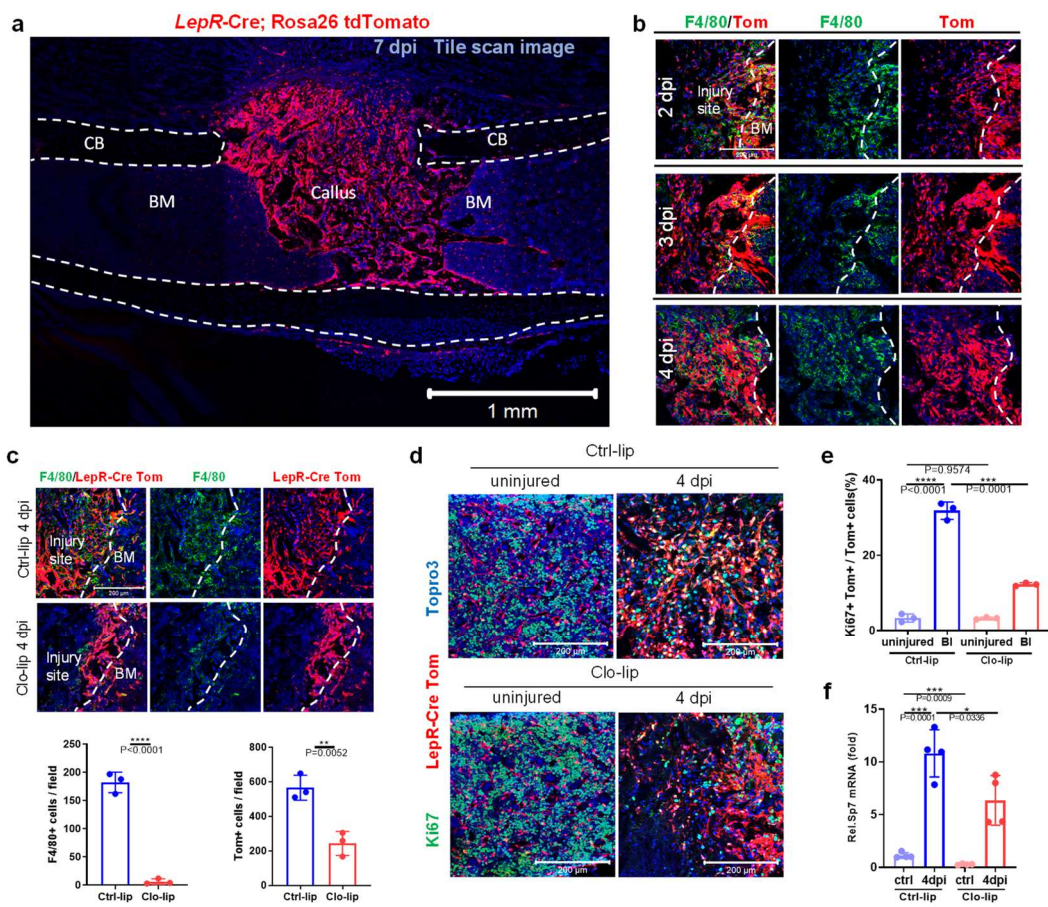


**Figure. S2 Osteodirective Mφs support the proliferation and differentiation of stromal cells.**

**(a)** Immunofluorescent analysis of Tomato(+) cells in *LepR*-Cre; tdTomato mice at the bone injury sites at 7 dpi. Dash lines indicate the cortical bone surface.

**(b)** Immunofluorescent analysis of F4/80(+) cells in *LepR*-Cre; tdTomato mice in the bone injury sites at 2, 3 and 4 dpi. Dash lines indicate the boundary between injury site and uninjured bone marrow.

**(c)** Immunofluorescent analysis of F4/80(+) cells in *LepR*-Cre; tdTomato mice in the bone injury sites at 4 dpi following treatment with Ctrl-lip and Clo-lip. The number of F4/80(+) cells (left) and Tomato(+) cells (right) at the bone injury sites at 4 dpi treated with Ctrl-lip and Clo-lip, n = 3. Dash lines indicate the boundary between injury site and uninjured bone marrow.

**(d)** Immunofluorescent analysis of Ki67(+) cells in *LepR*-Cre tdTomato mice at the bone injury site at 4 dpi and in the uninjured bone marrow area of the diaphysis following Ctrl-lip and Clo-lip treatment.

**(e)** Percentage of Ki67(+) *LepR*-Cre-labeled Tomato(+) cells among all Tomato(+) cells at the bone injury sites and in the uninjured area at 4 dpi following Ctrl-lip and Clo-lip treatment, n = 3.

**(f)** Quantitative RT-PCR analyses of *Sp7* mRNA expression in bone tissues from bone injury sites (4 dpi) and from control uninjured region of contralateral tibiae following Ctrl-lip and Clo-lip treatment, n = 4.

Scale bars: 1 mm in (a), 200 μm in (b), (c) and (f). Data are shown in mean ± S.D. Statistical significance was determined by unpaired Student's t-tests. P- values are shown in each graph.





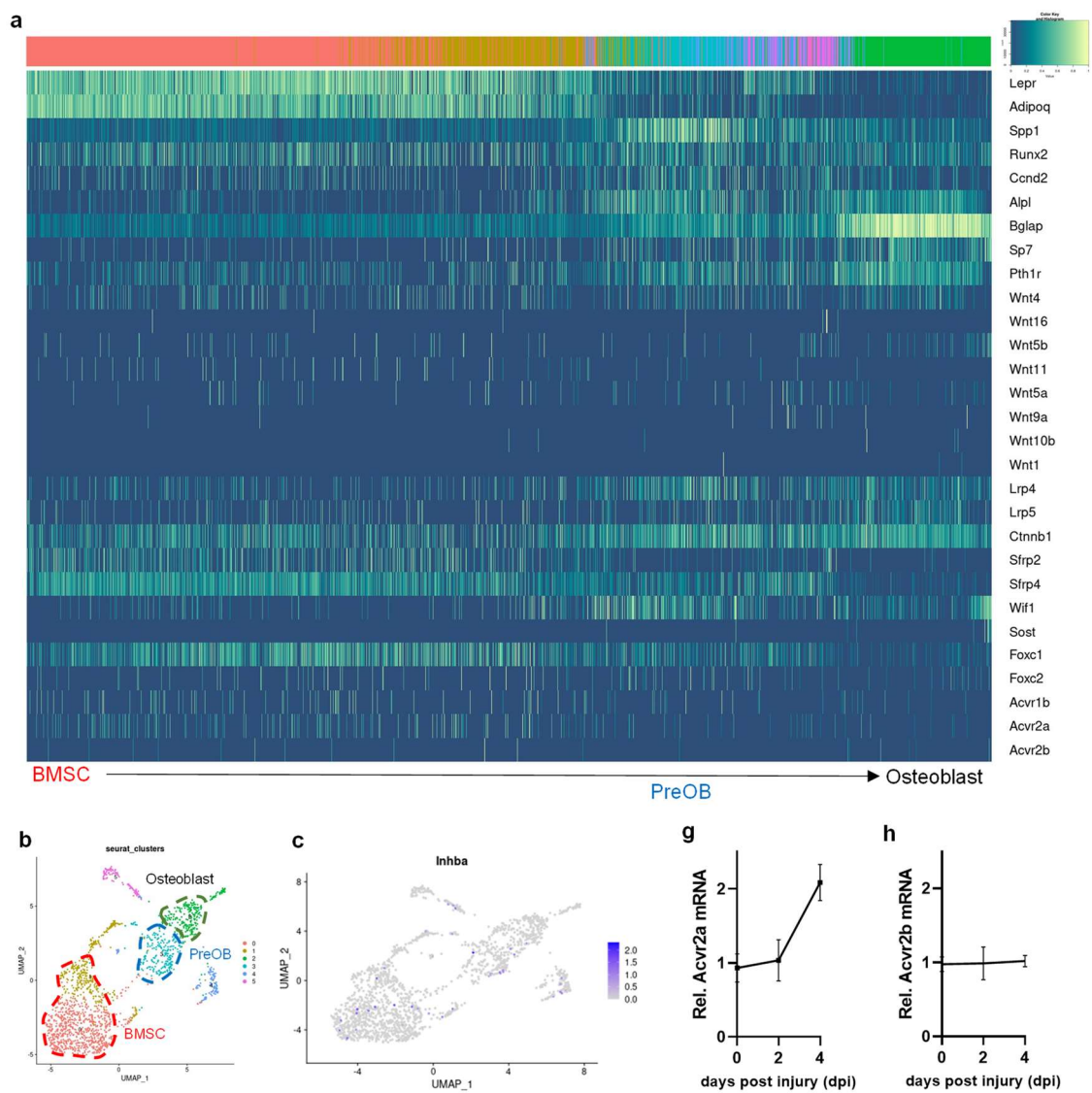
**Figure. S3 Presentative gene expression pattern in bone marrow F4/80(+) and Csf1r(+)**

**cells.**

**(a)** Heatmap pf top5 marker genes that were differentially expressed in each cluster.

**(b)** Expression patterns of osteogenic factor encoding genes *Bmp2* and *Osm* (encoding Oncostatin M) in the UMAP visualization. The dashed line enclosed macrophage-lineage clusters.





118

119

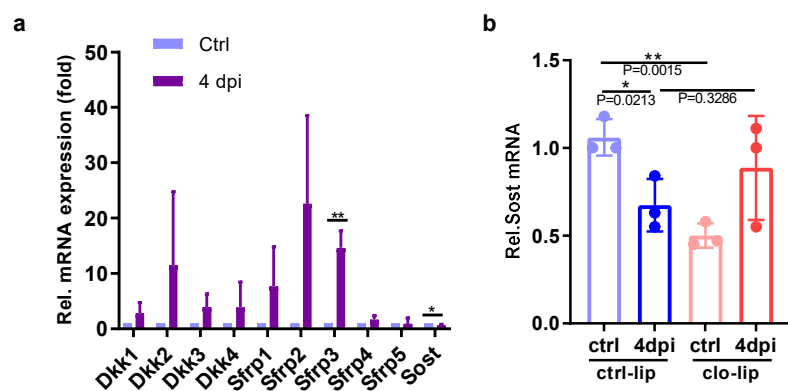
**Figure. S4 The source of activin A production.**

**(a)** Heatmap of representative pseudotime-dependent genes from single-cell RNA-seq analyses of *Cxcl12*-CreERT2; tdTomato (+) cells isolated from femurs at 14 days after bone marrow ablation (GSE136973).

**(b)** UMAP visualization of 6 clusters using Seurat, highlighting three major classes of osteoblastic cells.

**(c)** Expression patterns of *Inhba* in the UMAP visualization.

**(d, e)** Quantitative RT-PCR analyses of *Acvr2a* and *Acvr2b* mRNA expression in bone tissues from bone injury sites at 0, 2, and 4 dpi, (n = 3 - 4 mice per each group).



147

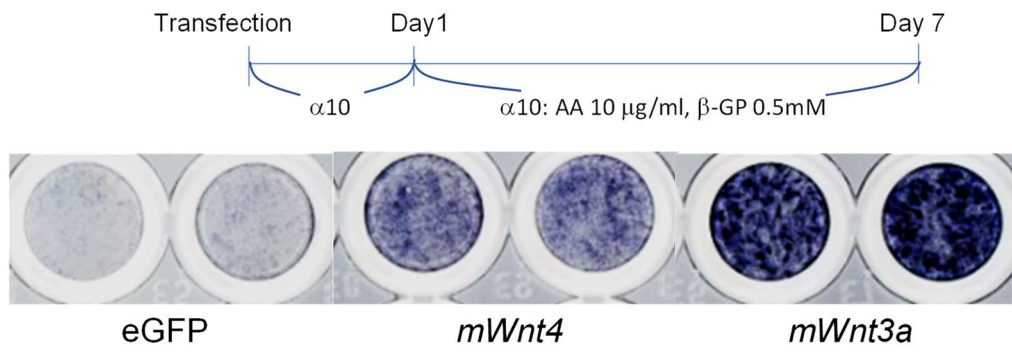
148

**Figure. S5 Wnt inhibitors gene expression in bone repair.**

**(a)** Quantitative RT-PCR analyses of Wnt inhibitors including *Dkk1* to 4, *Sfrp1* to 5 and *Sost* mRNA expression in bone tissues from bone injury sites (4 dpi) and uninjured region of contralateral tibiae (ctrl at 4dpi). n = 3 mice per each group.

**(b)** Quantitative RT-PCR analyses of *Sost* mRNA expression in bone tissues from bone injury sites (4 dpi) and uninjured region of contralateral tibiae (ctrl at 4dpi) treated with Ctrl-lip and Clo-lip (n = 4 mice per each group).

C3H10T1/2 cells



178 **Figure. S6 Wnt4 overexpression induced osteoblastogenesis in C3H10T1/2 cells.**  
179 Detection of ALP activity of C3H10T1/2 cells after transfection by eGFP, mWnt4 and mWnt3a  
180 for 24 hours, and cultured in 96-well-plate for 7 days.  
181  
182